DECTEROV, S.A., JUNG, I.-H., JAK, E., KANG, Y.-B., HAYES, P., and PELTON, A.D. Thermodynamic modelling of the Al_2O_3-CaO-CoO-CrO-Cr_2O_3-FeO-Fe_2O_3-MgO-MnO-NiO-SiO_2-S system and applications in ferrous process metallurgy. *VII International Conference on Molten Slags Fluxes and Salts,* The South African Institute of Mining and Metallurgy, 2004.

Thermodynamic modelling of the Al_2O_3-CaO-CoO-CrO-Cr_2O_3-FeO-Fe_2O_3-MgO-MnO-NiO-SiO_2-S system and applications in ferrous process metallurgy

S.A. DECTEROV*, I.-H. JUNG, E. JAK†, Y.-B. KANG**, P. HAYES†, and A.D. PELTON
**Centre de Recherche en Calcul Thermochimique, École Polytechnique de Montréal, Montréal, Quebec, Canada*
†The University of Queensland, Brisbane, Australia
***Department of Materials Science and Engineering, Pohang University of Science and Technology, Pohang, Korea*

Computerized thermodynamic databases for solid and liquid metal, slag and solid oxide phases in the Al_2O_3-CaO-CoO-CrO-Cr_2O_3-FeO-Fe_2O_3-MgO-MnO-NiO-SiO_2-S system have been developed by critical evaluation/optimization of all available phase equilibrium and thermodynamic data. The databases contain parameters of models specifically developed for molten slags, liquid steel and solid oxide solutions such as spinels, pyroxenes, olivine, monoxide (wustite, periclase, lime), corundum, etc. By means of the optimization process, model parameters are found which reproduce all thermodynamic and phase equilibrium data within experimental error limits. Furthermore, the models permit extrapolation into regions of temperature and composition where data are not available.

The databases are automatically accessed by user-friendly software that calculates complex equilibria involving simultaneously slag, metal, refractories and gases, for systems with many components, over wide ranges of temperature, oxygen potential and pressure.

A short review of the available databases is presented. The critical evaluation/optimization procedure is outlined using the Al_2O_3-CaO-FeO-Fe_2O_3-SiO_2 and Al_2O_3-CaO-MnO-SiO_2 systems as examples.

Several applications of the databases to deoxidation of iron and to inclusion control in steel are discussed.

Keywords: thermodynamics, phase equilibrium, phase diagrams, databases, ferrous metallurgy, steelmaking, inclusion control, slags, oxide systems.

Introduction

In recent years, thermodynamic modelling has been actively pursued apace with the improvement of computational techniques and software. Based on a proper thermodynamic model for every phase of a given system, all available thermodynamic and phase equilibrium data for a system are critically evaluated simultaneously in order to obtain one self-consistent set of model equations for the Gibbs energies, which best reproduce the data for all phases as functions of temperature and composition. This technique has come to be known as thermodynamic 'optimization'. Where data are lacking for a multicomponent system, the models and optimized model parameters for low-order (binary and ternary) subsystems can be used to provide good estimates.

In this way, the thermodynamic databases are developed. The databases are then used, along with Gibbs energy minimization software, to calculate multicomponent phase equilibria of importance for various applications. Over the last four years, several databases have been developed by the authors with the view to facilitate simulations of industrial processes in iron- and steelmaking.

In this article, we shall outline the technique of database development by critical evaluation/optimization. The chemical system that has been critically evaluated for applications in iron- and steelmaking will be briefly reviewed to give an idea of the major phases and phase equilibria in this system. Finally, several examples will be presented in order to demonstrate the versatility and accuracy of the developed thermodynamic databases to calculations of importance to inclusion engineering.

Thermodynamic databases

The selection of proper databases for a given system is a prerequisite for accurate thermodynamic calculations. The databases must be thermodynamically self-consistent; otherwise very erroneous results can often occur.

The FACT databases[1] for multicomponent oxide, salt, alloy and aqueous solutions have been developed by critical evaluation/optimization over the last 25 years. The databases contain over 4 400 compounds and 120 non-ideal multicomponent solution phases. The FACT databases were used for the calculations presented in the present article.

The FACT oxide solution database contains critically evaluated thermodynamic data for the molten slag phase and for many extensive oxide solid solutions containing the following components: Al_2O_3, As_2O_3, B_2O_3, CaO, CoO, CrO, Cr_2O_3, Cu_2O, FeO, Fe_2O_3, GeO_2, K_2O, Na_2O, MgO, MnO, NiO, PbO, SiO_2, SnO, TiO_2, Ti_2O_3, ZnO, and ZrO_2. Not all possible combinations of these components have

been critically evaluated. Generally, the critical assessment and optimization of model parameters have been done for certain subsystems of this 23-component system, which are of particular importance for various applications in materials science, ceramics, geology, petrochemistry, corrosion, metallurgy (pyro-, hydro-, electro-), combustion, energy, glass technology, etc.

The molten slag phase is modelled by the Modified Quasichemical Model[2–4] in which short-range-ordering is taken into account. Ceramic solid solutions are mainly modelled in the framework of the Compound Energy Formalism[5], taking into account the crystal structure and physical nature of each solution. For example, the model for spinel[6] describes the distribution of cations and vacancies over tetrahedral (T) and octahedral (O) sites: $(Al^{3+}, Co^{2+}, Co^{3+}, Cr^{2+}, Cr^{3+}, Fe^{2+}, Fe^{3+}, Mg^{2+}, Ni^{2+}, Zn^{2+})^{T}[Al^{3+}, Co^{2+}, Co^{3+}, Cr^{3+}, Fe^{2+}, Fe^{3+}, Mg^{2+}, Ni^{2+}, Zn^{2+}, Va]_2^{O}O_4$. The olivine solution is modelled by considering two octahedral sites: $[Ca^{2+}, Co^{2+}, Fe^{2+}, Mg^{2+}, Mn^{2+}, Ni^{2+}, Zn^{2+}]^{M2}(Ca^{2+}, Co^{2+}, Fe^{2+}, Mg^{2+}, Mn^{2+}, Ni^{2+}, Zn^{2+})^{M1}SiO_4$, and the mixing of cations on three sublattices was taken into account for melilite and pyroxenes.

The solubilities of S, SO_4, PO_4, CO_3, H_2O, OH, F, Cl, Br and I in molten slags were modelled by the Blander-Reddy Capacity Model[7,8]. In this model, dissolved anions such as S^{2-} are assumed to form ideal solutions, substituting for O^{2-} and SiO_4^{4-} anions in the silicate slag. From this simple assumption, sulfide, sulfate, etc. solubilities (capacities) can be predicted with good accuracy[7]. Because the thermodynamic model used for each phase in the FACT database has been chosen with consideration of the actual structure of the phase, the predictive ability is very high for estimating the properties of multicomponent solutions.

Recently, a new FACT database for liquid steel was developed based on a new Associate Model[9] to accurately describe deoxidation phenomena in liquid steel. This database has been developed for 15 deoxidation systems Fe-M-O (M = Al, B, Ba, Ca, Ce, Cr, La, Mg, Mn, Nb, Si, Ta, Ti, V, Zr)[9], and has high predictive ability for multicomponent systems. The calculation of deoxidation equilibria in steel will be illustrated below in more detail.

A complete 14-element (Fe-Al-C-Co-Cr-Mn-Mo-N-Nb-Ni-Si-Ti-V-W) FACT database for steel alloys will also soon be available. This database contains fully assessed data for alloy and carbonitride phases: liquid, fcc, bcc, hcp, cementite, laves phase, carbides, sigma phase, etc. This database is an updated[10] version of the SGTE solution database[11]. All solutions in the database were modelled using the Compound Energy Formalism.

The Gibbs energy minimization software of the FactSage[1] thermochemical computing system was used to perform the thermodynamic calculations in this work. The FACT databases discussed above are automatically accessed by this user-friendly software. Users can perform complex equilibrium calculations involving simultaneously, slag, steel, inclusions, refractories and gases, for systems with many components, over wide ranges of temperature, oxygen potential and pressure.

Oxide database development for ferrous process metallurgy

Thermodynamic databases are prepared by the following thermodynamic 'optimization' procedure:

- For each particular solution, an appropriate model is developed, which is based upon the physical nature and structure of the solution. The model gives the functional dependence of the thermodynamic properties of the solution on temperature and composition.
- Then, one set of self-consistent parameters of the models is obtained for all phases in a chemical system of interest. All available thermodynamic and phase equilibrium data from the literature are critically evaluated and used to select model parameters. Through the use of FactSage calculations, discrepancies in the available data often become evident and can be resolved. Interpolations and extrapolations can be made in a thermodynamically correct manner. When the crucial data are not available or the contradictions between various sets of data cannot be resolved, our experimentalist collaborators are asked to make a few experiments at selected temperatures and compositions to constrain the models. This is done for all 2-component, 3-component (and, if data are available, higher-order) subsystems of a given chemical system.
- Next, the models are used to estimate the thermodynamic properties of the N-component solutions from the database of parameters for lower-order subsystems. Finally, multicomponent phase equilibria are calculated for simulation of industrial processes.

Over the last several years, these techniques have been applied systematically to the evaluation of dozens of oxide systems of importance to iron- and steelmaking. In this way, the vast amount of thermodynamic data amassed over the past decades is being critically evaluated and correlated, extended to the prediction of properties of multicomponent solutions, and made readily available to the industrial and academic communities.

The six-component system Al_2O_3-CaO-FeO-Fe_2O_3-MgO-SiO_2, which is important for most applications of the oxide database, has been completely re-optimized using the new powerful models developed for the liquid slag and multicomponent solid solutions such as spinel, pyroxenes, olivine, melilite, monoxide, etc. Parameters of the models have been optimized to represent many thousands of experimental points. All this experimental information from thousands of publications has been critically evaluated, made self-consistent and condensed to several dozens model parameters in the oxide database. New models have made it possible to reproduce all experimental data within experimental error limits from 25°C to above the liquidus temperatures at all compositions and oxygen partial pressures from saturation with metals to equilibrium with oxygen.

In a single article it is not possible to give even a brief overview of all thermodynamic and phase equilibrium data that have been taken into account. Figures 1 to 11 present a series of calculated phase diagrams along with experimental data points for binary and ternary subsystems of the Al_2O_3-CaO-FeO-Fe_2O_3-SiO_2 systems which are of most importance to ferrous and non-ferrous process metallurgy. The optimized phase diagrams for the Al_2O_3-CaO-SiO_2 system and its binary subsystems and for the Fe-O system have been published elsewhere[6,12]. These figures give an idea of the major phases and phase equilibria in the Al_2O_3-CaO-FeO-Fe_2O_3-SiO_2 system over the whole range of oxygen potentials from metal saturation to equilibrium with air. The typical scatter of experimental data and the accuracy of model calculations are also obvious from the figures. In particular, the liquidus in the fayalite and

calcium ferrite slag regions is reproduced within experimental error limits, as can be seen from Figures 9 to 11. Of course, many other types of data, such as all thermodynamic properties, activities, Fe^{2+}/Fe^{3+} ratios, distributions of cations between different sublattices in solid solutions, partial pressures of equilibrium gaseous species, etc., have also been reproduced and can be calculated and plotted by the software. It is the internal contradiction between these other thermodynamic data and experimental phase diagrams that causes the apparent disagreement of the calculated and experimental phase boundaries in a few cases (see, e.g., Figures 3 and 7). The wustite liquidus in Figure 3 must also go through a minimum at a congruent melting point to produce thermodynamically correct topology of the phase diagram, which seems to be in disagreement with the experimental data points.

Several other components, MnO, CrO, Cr_2O_3, NiO, CoO, etc., have been added to the six-component system Al_2O_3-CaO-FeO-Fe_2O_3-MgO-SiO_2 over the range of composition, temperature and oxygen partial pressure, which is important for ferrous process metallurgy.

In particular, the Al_2O_3-CaO-MnO-SiO_2 system has been optimized. This system is of interest for inclusion control in Mn/Si-killed steel, as will be discussed in more detail below. The phase equilibria in this quaternary system are illustrated by Figures 12 to 19. The optimized phase diagrams for the MnO-CaO and MnO-SiO_2 binary subsystems have been published elsewhere[47,48]. These figures demonstrate how thermodynamic models describe simultaneously phase diagrams (Figures 12 and 16), thermodynamic properties (Figure 13), activities (Figures 14 and 17) and slag-alloy phase equilibria (Figure 18). Of course, a great number of other experimental data points have also been reproduced. Figures 15 and 19 present the calculated phase diagrams of all ternary subsystems and one section through the quaternary system, which are

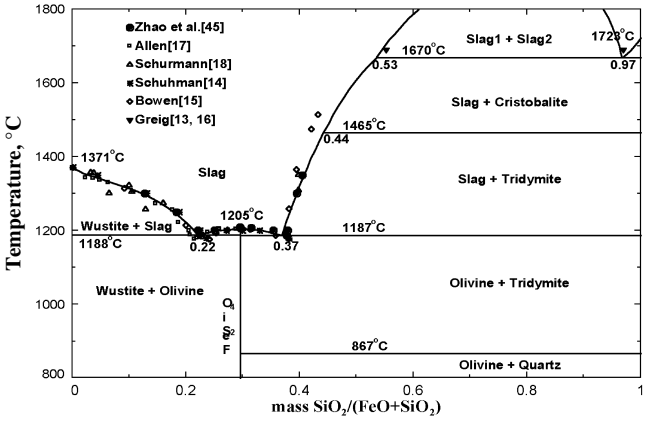

Figure 1. Calculated (optimized) Fe-Si-O phase diagram in equilibrium with iron

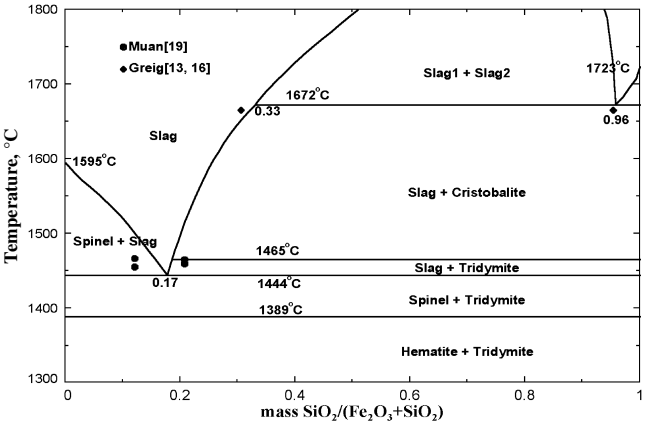

Figure 2. Calculated (optimized) Fe-Si-O phase diagram in equilibrium with air

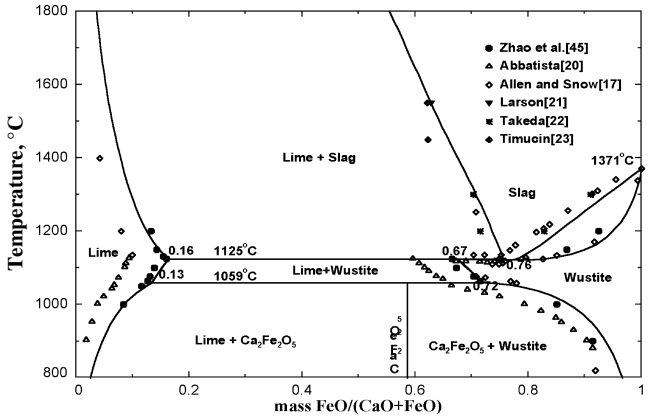

Figure 3. Calculated (optimized) Ca-Fe-O phase diagram in equilibrium with iron

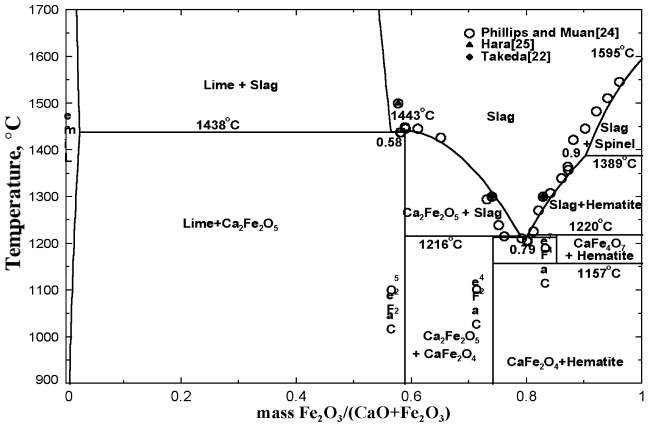

Figure 4. Calculated (optimized) Ca-Fe-O phase diagram in air

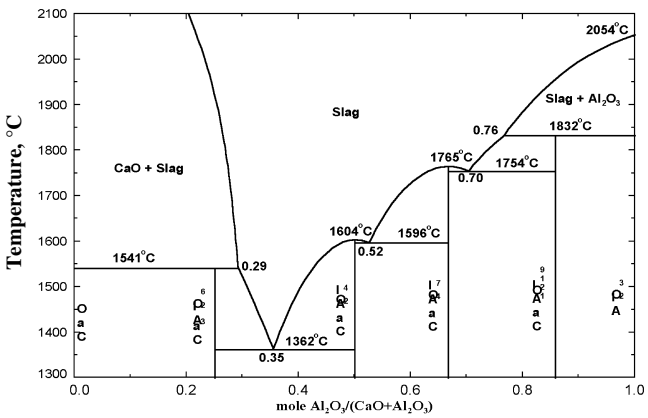

Figure 5. Calculated (optimized) CaO-Al_2O_3 phase diagram

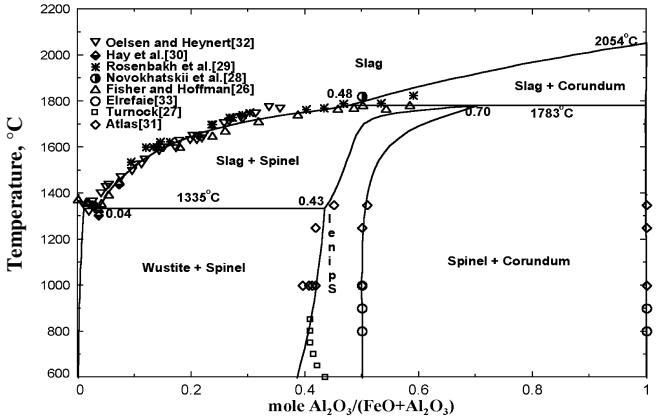

Figure 6. Calculated (optimized) FeO-Al_2O_3 phase diagram in equilibrium with iron

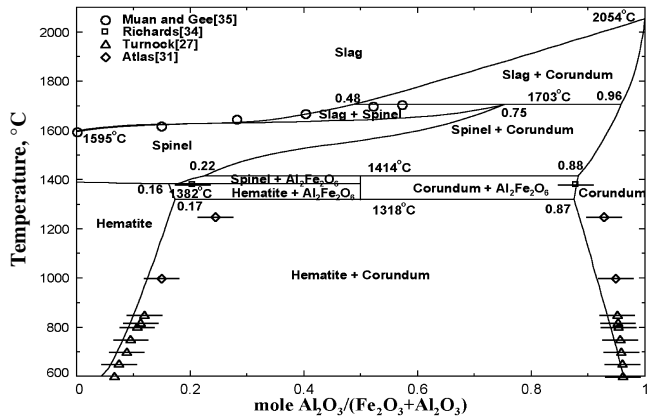

Figure 7. Calculated (optimized) Al-Fe-O phase diagram in equilibrium with air

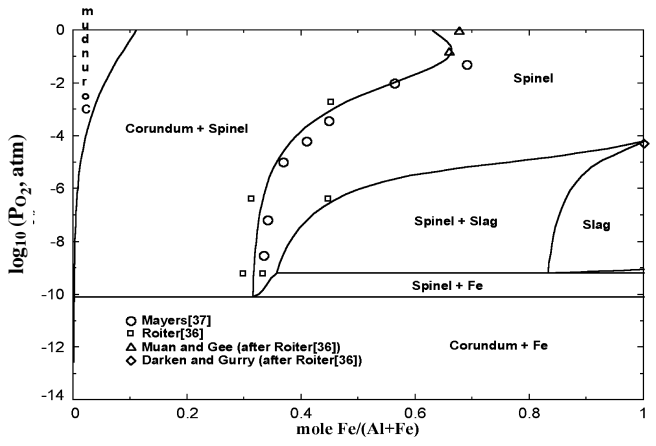

Figure 8. Calculated (optimized) Al-Fe-O phase diagram at 1500°C

consistent with thermodynamic laws and with all experimental information available for this quaternary system. Similarly, the thermodynamic databases that have been developed make it possible to calculate any other phase diagram section even for regions of composition and temperature where no experimental data are available.

Applications of thermodynamic databases to inclusion engineering

Inclusion control is the key to the production of high clean

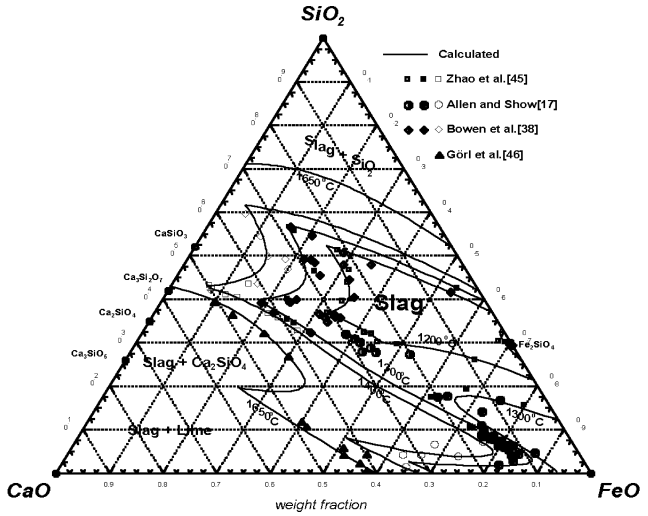

Figure 9. Calculated liquidus of the Ca-Fe-Si-O system in equilibrium with iron at temperatures between 1200°C and 1650°C compared with experimental data[17,38,45,46]

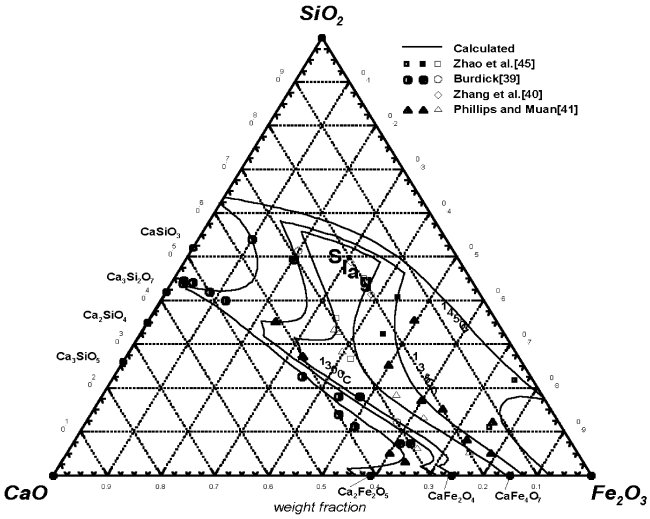

Figure 10. Calculated liquidus of the Ca-Fe-Si-O system in equilibrium with air at temperatures between 1300°C and 1450°C compared with experimental data[39–41,45]

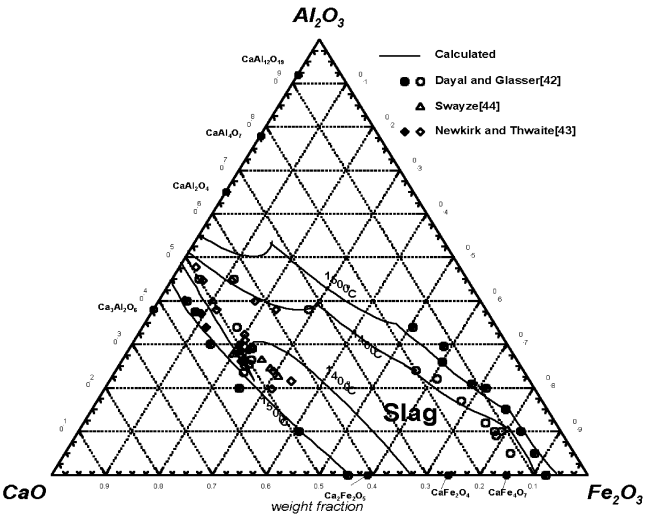

Figure 11. Calculated liquidus of the Al-Ca-Fe-O system in equilibrium with air at 1400°C and 1500°C compared with experimental data[42–44]

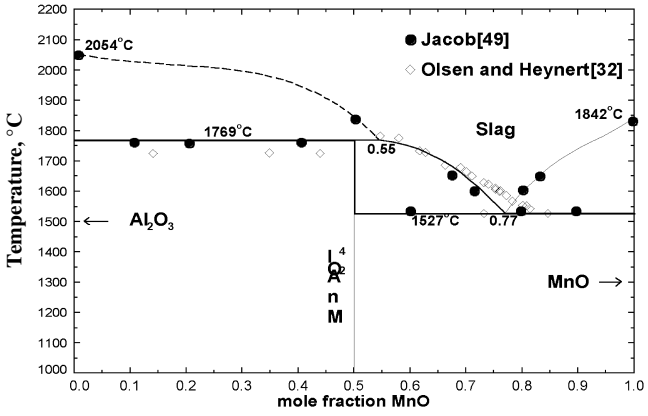

Figure 12. Calculated (optimized) $MnO-Al_2O_3$ phase diagram

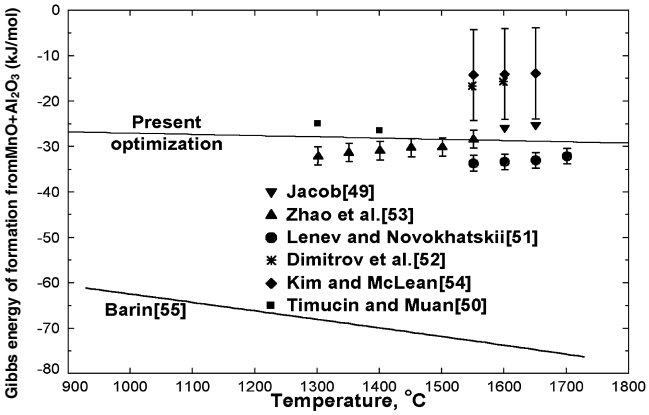

Figure 13. Optimized Gibbs energy of formation of $MnAl_2O_4$ from solid MnO and Al_2O_3

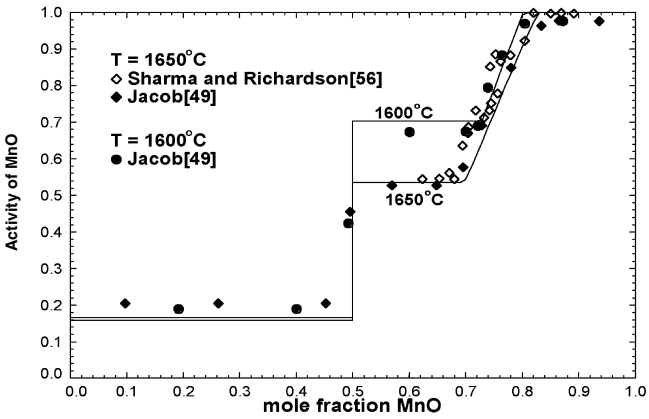

Figure 14. Calculated (optimized) activity of MnO (with respect to solid standard state) in the $MnO-Al_2O_3$ system at 1600°C and 1650°C

or ultra-high clean steel. Inclusions appear in steel at various stages of its production and cause serious problems: nozzle clogging, breakage of steel wire during drawing, hydrogen induced cracking (HIC), low-temperature embrittlement, fatigue failure, degradation of surface quality, and so on. Inclusions are mainly formed either during the deoxidation process, or by slag entrapment, breakdown of refractory materials and reoxidation by air. Inclusions can also precipitate due to changes of solubility, which occur as temperature decreases.

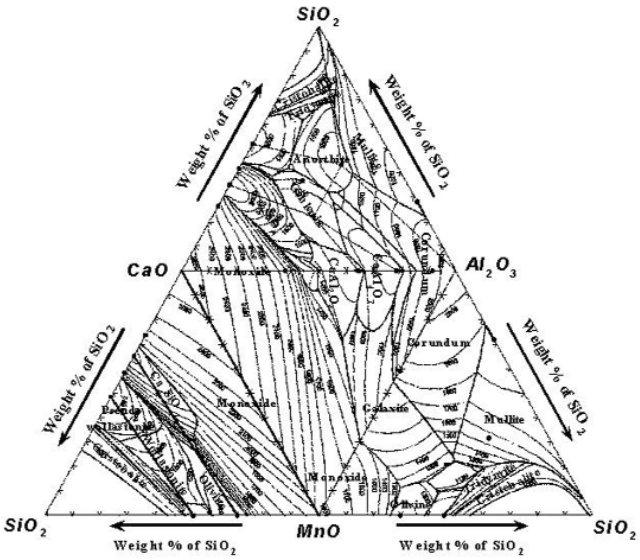

Figure 15. Liquidus surfaces of the four ternary subsystems of the $CaO-MnO-SiO_2-Al_2O_3$ system calculated from the thermodynamic models (temperature in °C)

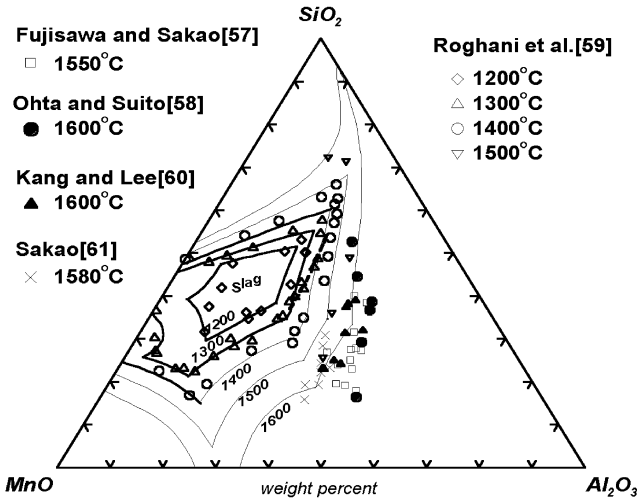

Figure 16. Calculated liquidus of the $MnO-Al_2O_3-SiO_2$ system at temperatures between 1200°C and 1600°C compared with experimental data. Dashed line is calculated metastable liquidus of Al_2O_3 (corundum) at 1300°C

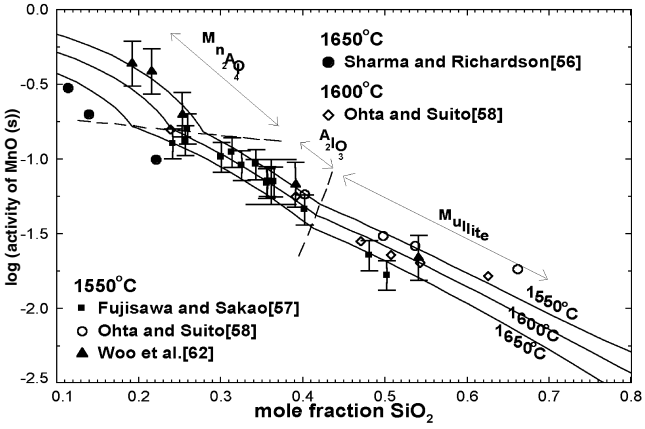

Figure 17. Calculated activities of MnO (solid standard state) in $MnO-Al_2O_3-SiO_2$ liquid slags at 1550°C, 1600°C and 1650°C at saturation with solid $MnAl_2O_4$, Al_2O_3 or mullite

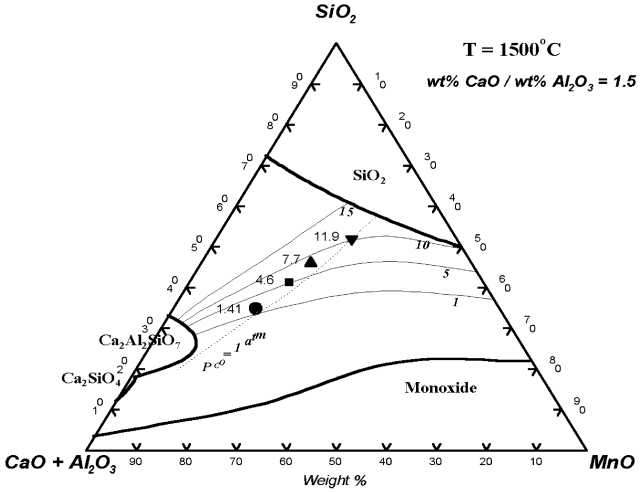

Figure 18. Calculated composition of CaO-MnO-SiO_2-Al_2O_3-(FeO) liquid slag with a CaO/Al_2O_3 weight ratio of 1.5 in equilibrium with C-saturated Fe-Mn-Si-C alloy containing 11 wt% Fe and indicated constant weight percent Si at 1500°C. Dashed line is the calculated composition of the liquid slag in equilibrium with the manganese alloy and a gas phase with P_{CO} = 1 atm. Experimental points of Ding and Olsen[63] at P_{CO} = 1 atm are also shown. The calculated FeO content of the slag is less than 0.01 weight percent

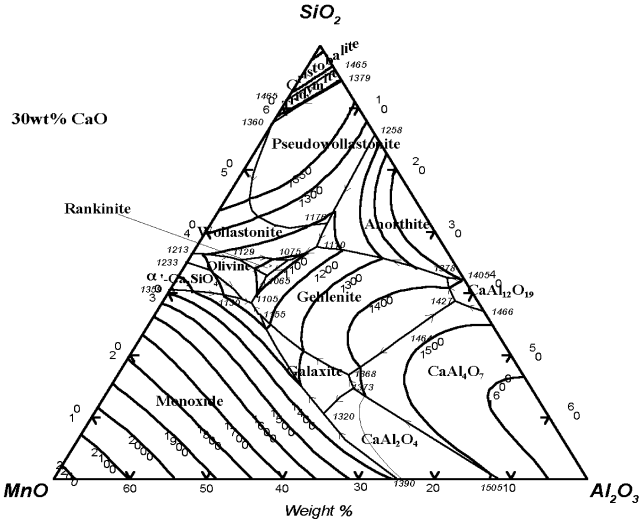

Figure 19. Predicted liquidus surface of the CaO-MnO-S_iO_2-Al_2O_3 system at 30 wt% CaO

Inclusions can be floated and captured by top slags in secondary steelmaking processes. However, the removal of inclusions is very limited during these processes due to the short process time and to the continuous circulation of liquid steel in the ladle. Therefore, the control of the composition of inclusions has become crucial in modern steelmaking processes. That is, since the presence of inclusions cannot be avoided, it is important to modify their composition to render them less harmful. Because, thermodynamically, the composition of inclusions is very sensitive to the concentrations of even dilute elements dissolved in the steel, accurate thermodynamic data for both steel and inclusions are indispensable to the development of inclusion engineering technology.

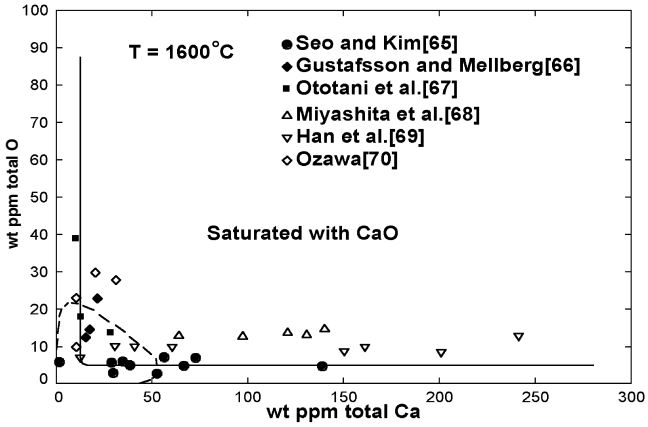

Figure 20 Total dissolved oxygen and total dissolved Ca contents of liquid Fe in equilibrium with solid CaO. Lines calculated from the database with the Associate Model[9]. Dashed line calculated from Wagner formalism with parameters of JSPS[71]

In this section, a few examples will be presented in order to demonstrate the versatility and accuracy of the thermodynamic databases that have been developed for calculations of importance to inclusion engineering. Some additional examples have recently been reported by Jung *et al*.[64].

Ca deoxidation: the Fe-Ca-O system

Figure 20 shows the calculated deoxidation curve in the Fe-Ca-O system at 1600°C compared with experimental data[65–70]. In the Associate Model[9], the liquid iron is assumed to contain dissolved unassociated Ca and O atoms as well as molecules (associates) CaO. The curves in Figure 20 were calculated using the Associate Model with one temperature-independent parameter, which is the Gibbs energy Δg_{CaO} for the association reaction Ca + O = CaO.

The shape of the calculated Ca deoxidation curve in Figure 20 may be explained as follows. Because Δg_{CaO} is very negative, the association reaction is displaced very strongly to the right. Hence, a solution will contain either dissolved CaO and O species (but virtually no Ca species), or dissolved CaO and Ca species (but virtually no O species). Suppose we start with Fe containing a high concentration of dissolved oxygen at 1600°C and begin adding Ca. At first the Ca reacts with the oxygen to form CaO associates, leaving virtually no free Ca in solution. When the concentration of CaO reaches ~ 17 ppm it attains equilibrium with solid CaO: CaO = CaO(s).

As more Ca is added to the metal, it reacts with dissolved oxygen to precipitate solid CaO; the concentration of dissolved oxygen thus decreases, while the concentration of CaO remains constant (and hence the concentration of total dissolved Ca remains nearly constant). This results in the nearly vertical section of the deoxidation curve in Figure 20. When the total dissolved oxygen content has been reduced to ~ 5 ppm, the concentrations of free dissolved O and Ca are both extremely low, and CaO associates are virtually the only species in solution. Further addition of Ca thus serves only to increase the free Ca concentration, with virtually no further precipitation of CaO; hence the nearly horizontal section of the curve in Figure 20.

Several authors[65,66,71–74] have attempted to model the Ca deoxidation curve using the classical Wagner formalism

without considering the formation of associates. Very large negative temperature-dependent first- and second-order interaction parameters ε_{Ca}^{O}, ρ_{Ca}^{O}, $\rho_{Ca}^{Ca,O}$ were required. Furthermore, most authors also had to arbitrarily adjust the equilibrium constant K_{CaO} for the formation of solid CaO by two or three orders of magnitude from its literature value in order to fit the data. In the present calculations, this was not necessary, and accepted literature values were used as recommended by Turkdogan[75]. The calculated solubility (deoxidation) curves by other authors all have strange shapes, some with minima and maxima, and even one in the form of a circle[66]. The model of JSPS[71] is the most widely used; the 'deoxidation curve' calculated from this model, and reported in the literature, is shown in Figure 20 by the dashed line. We have shown[9] that this is actually an unstable solution of the interaction parameter formalism; the true stable solution actually lies at extremely low (< 0.01 ppm) Ca and O contents. Hence, we believe that the present calculations elucidate the deoxidation behaviour of Ca for the first time.

Al deoxidation: the Fe-Al-O system

The deoxidation curves from several selected authors[76–81] are shown in Figure 21. In the Associate Model[9], the liquid iron is assumed to contain dissolved unassociated Al and O atoms as well as associates AlO and Al_2O.

In a very dilute solution, unassociated Al and O predominate. Therefore, the deoxidation reaction may be written as $2Al + 3O = Al_2O_3$ (solid). From the equilibrium constant of this reaction, one would expect the oxygen content to decrease continuously as the dissolved Al content increases. This is indeed the case for low Al contents where most of the oxygen is dissolved as free O.

However, at higher Al contents, most of the dissolved oxygen is in the form of AlO associates because the equilibrium constant of reaction $Al + O = AlO$ is very large, and the principal deoxidation equilibrium becomes $3AlO = Al_2O_3$ (solid) + Al. From the equilibrium constant of this reaction, one can deduce that an increase in the total dissolved Al content now results in an increase in X_{AlO} and thus in an increase in total dissolved oxygen. Hence, a 'deoxidation minimum' is observed in the curves of Figure 21. (Note that the axes in Figure 21 give the total dissolved Al (as Al+AlO+$2Al_2O$) and the total dissolved oxygen (as O+AlO+Al_2O).) Therefore, in general, if the Gibbs energy of formation of the associates is sufficiently negative, a deoxidation minimum will be observed for a deoxidant M whenever the deoxidation product M_xO_y has a ratio (y/x) > 1.

The Gibbs energies of reactions $Al + O = AlO$ and $2Al + O = Al_2O$ were optimized to reproduce the experimental data. The curves in Figure 21 are calculated from these parameters. Although the parameters are constant, independent of temperature, the temperature dependence of the data is very well reproduced by the model.

It can easily be shown that the assumption of the higher associate Al_2O only has a visible effect on the calculated curves when log[wt% total Al] > -0.3. Even at higher Al concentrations, an acceptable fit can be obtained without considering the formation of Al_2O.

Previously, Sigworth and Elliott[82] modelled this system using the Wagner interaction parameter formalism without considering the formation of associates. A very negative parameter ε_{Al}^{O} was required, with a temperature dependence chosen to fit the data. The deoxidation equilibrium at 1600°C, calculated by their model, is shown in Figure 21 by the dashed line. Clearly, their model cannot be extrapolated outside the composition range of the data. On the other hand, with the present model, extrapolations both in composition and temperature are reasonable.

Modification of solid Al_2O_3 inclusions to liquid CaO-Al_2O_3 inclusions: The Fe-Al-Ca-O system

Solid Al_2O_3 inclusions formed during the Al deoxidation process are not easily removed by floating in the secondary refining process, and thereafter they may degrade the mechanical properties of the steel as well as cause nozzle clogging. In order to reduce these harmful effects, Ca treatment technology is often used, by which solid Al_2O_3 inclusions are modified to less harmful liquid CaO-Al_2O_3 inclusions. The globular liquid inclusions can float more easily to the top slag in the secondary steelmaking process and are less likely to become attached to the nozzle wall. In order to understand the Ca treatment process, an inclusion diagram for the Fe-Al-Ca-O system is essential.

Figure 22 presents the inclusion diagram for the Fe-Al-Ca-O system at 1600°C calculated using the thermodynamic databases. The equilibrium deoxidation products are also indicated on the diagram and the phase

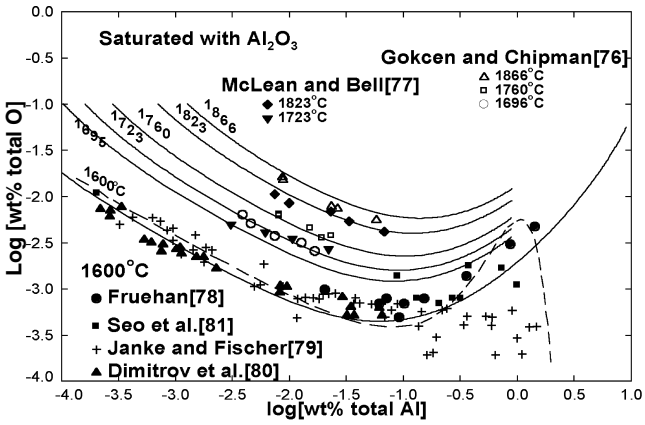

Figure 21. Total dissolved oxygen and total dissolved Al contents of liquid Fe in equilibrium with solid Al_2O_3. Lines calculated from the database with the Associate Model.[9]. Dashed line calculated from Wagner formalism with parameters of Sigworth and Elliott[82]

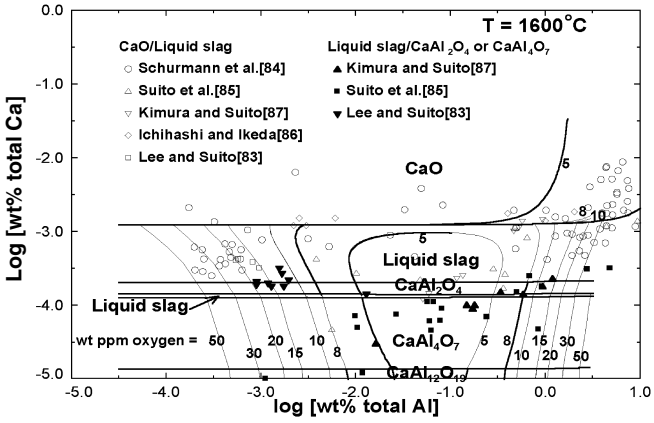

Figure 22. Calculated inclusion diagram for complex deoxidation with Ca and Al showing total dissolved oxygen content of liquid steel and equilibrium deoxidation products as functions of total dissolved Ca and Al

boundaries are represented as heavy lines. Iso-oxygen content lines from 5 to 50 wt ppm oxygen are also plotted. Each point on the diagram represents an equilibrium of liquid steel with one or two oxide phases. That is, if oxygen is progressively dissolved in the liquid iron containing certain amounts of Al and Ca (as given by the axes of the diagram), then an oxide phase indicated on the diagram will precipitate when a certain oxygen content is reached. The latter can be estimated from the iso-oxygen lines. Since the oxide phases contain a very small amount of iron under these conditions, their compositions are close to the CaO-Al_2O_3 system. As can be seen from Figure 5, there are two slag regions at 1600°C on both sides of the $CaAl_2O_4$ compound. Since $CaAl_2O_4$ melts congruently at ~1604°C, a similar diagram calculated above 1604°C would not contain the $CaAl_2O_4$ region. Similarly, since the $CaAl_2O_4$-$CaAl_4O_7$ eutectic temperature is ~1596°C, a diagram calculated below 1596°C would not contain the lower 'liquid slag' region.

A deoxidation minimum is clearly seen near log [wt% Al] ~ -1.2 (i.e. at Al concentration of about 500 wt ppm) similar to Figure 21. It can be seen that the equilibrium deoxidation product is nearly independent of Al content, depending only on the Ca content. When log[wt% total Ca] > -2.9 (i.e. total dissolved Ca > 13 ppm), solid CaO is the deoxidation product, and the oxygen content is ~5 wt ppm. At higher total Ca contents the oxygen content does not decrease substantially below 5 ppm. This behaviour can be understood with reference to the Ca deoxidation curve in the Fe-Ca-O system in Figure 20, where the nearly vertical and nearly horizontal branches of the deoxidation curve occur at ~13 wt ppm Ca and ~5 wt ppm O, respectively. In particular, the drastic change of the oxygen content in the steel after crossing the CaO+Slag equilibrium line at about 13 wt ppm Ca corresponds to the nearly vertical line in Figure 20.

Several authors[83–87] have measured the line along which solid CaO and liquid slag co-exist as well as the line along which either (slag+$CaAl_2O_4$) or (slag+$CaAl_4O_7$) co-exist. Measurements were performed in CaO crucibles in the first case, and Al_2O_3 crucibles in the second case. The data points are plotted on Figure 22. Within the large experimental scatter, these results confirm the model calculations.

The newly calculated inclusion diagram differs significantly from previous diagrams[65,88–91], in which the calculated phase boundaries slope upwards to the right.

The inclusion diagram can be applied to the Ca-treatment of Al_2O_3 solid inclusions. In order to modify the Al_2O_3 inclusions to the liquid CaO-Al_2O_3 phase, at least ~2 wt ppm Ca (i.e. log [wt% Ca] ~ -3.7) is necessary, but the Ca content should be less than ~13 wt ppm (log [wt% Ca] ~ -2.9) to prevent the formation of the solid CaO phase. It should be noted that although the Ca treatment for Al_2O_3 inclusions is useful to prevent nozzle clogging and to absorb inclusions in top slags, the lowest eutectic temperature in the CaO-Al_2O_3 binary system is still much higher than the temperature in the rolling process. Therefore, the CaO-Al_2O_3 inclusions will be solid and undeformable during the rolling process.

Formation of CaS inclusions during Ca treatment: the Fe-Al-Ca-Si-O-S system

During the Ca treatment process discussed above, the amount of sulfur in the liquid steel is very important because solid CaS is readily formed. CaS inclusions can be as harmful as solid Al_2O_3. Therefore, the Ca/S ratio in liquid steel should be closely controlled[92].

Figure 23 shows the calculated results for the simulation of CaSi(1:1) wire injection into 100 tonnes of liquid steel (iron containing 6, 30 and 500 wt ppm O, S and Al, respectively) with suspended Al_2O_3 inclusions. In the calculations, no losses of CaSi (as, for example, by the volatilization of Ca) are assumed. The amount of suspended Al_2O_3 inclusions is set at 100 wt ppm in Figure 23(a) and 300 wt ppm in Figure 23(b). As the CaSi wire is injected, initially solid Al_2O_3 is converted to solid $CaAl_{12}O_{19}$ and $CaAl_4O_7$ which contain very small amounts of iron. Thereafter, the liquid oxide inclusions, composed of CaO-Al_2O_3 with a small amount of CaS, are formed. As the amount of CaSi increases further, solid CaS and solid CaO inclusions begin to precipitate and eventually become predominant. In both Figure 23(a) and Figure 23(b), CaS is precipitated before CaO. The relative amounts of the solid phases depend on the initial amount of suspended Al_2O_3 inclusions. Clearly, more initial sulphur in the liquid steel will result in the precipitation of CaS at an earlier stage, even before the formation of the CaO-Al_2O_3 liquid if the sulphur content is large enough.

With the aid of such diagrams, the proper amount of CaSi injection can be calculated, as a function of initial contents of Al, S and suspended Al_2O_3, in order to form deformable liquid inclusions without forming harmful solid oxide or CaS inclusions.

Clearly, injection of CaSi is also useful for reducing to some extent the S content in steel. Calculated diagrams such as Figure 23 can also be used to determine the minimum S contents that can be attained without formation of harmful solid CaS inclusions.

Mn/Si deoxidized steel: MnO-Al_2O_3-SiO_2 inclusions

Mn/Si complex deoxidation is indispensable for the production of high value steel such as tire-cord steel and high-Ni steel (Fe-36%Ni Invar steel) in order to avoid the harmful effects of solid Al_2O_3 inclusions formed during Al deoxidation. Undeformable Al_2O_3 inclusions cause wire breakage during the wire-making process in tire-cord production. Therefore Mn/Si deoxidation, which results in inclusions of low melting temperature, is usually preferred. In actual plant processes, Mn/Si deoxidation usually results in liquid MnO-Al_2O_3-SiO_2 inclusions as deoxidation products. During the refining stage, these MnO-Al_2O_3-SiO_2 inclusions may react with CaO-containing top slags to become CaO-MnO-Al_2O_3-SiO_2 inclusions. In this study, the relationship between the Mn/Si ratio in the liquid tire-cord steel and the composition of the MnO-Al_2O_3-SiO_2 inclusions is elucidated with a view to forming inclusions with low melting temperatures.

Figure 24 shows the calculated compositional trajectories of the MnO-Al_2O_3-SiO_2 inclusions for various constant Mn/Si deoxidant ratios as Al content is varied in liquid tire-cord steel at 1600°C. (The carbon content in tire-cord steel, which is about 0.7 wt%, was ignored in the calculations.) The total amount of Mn and Si was set to 1.0 wt% and the calculated phase diagrams at 1600°C and 1200°C are superimposed on the figure. A small amount of FeO (less than 3 wt%) always exists in such inclusions and this was included with MnO (on a molar basis) in Figure 24. Phase boundaries measured[58,60] for various Mn/Si ratios are also shown in Figure 24. The agreement with the calculations is excellent.58,60

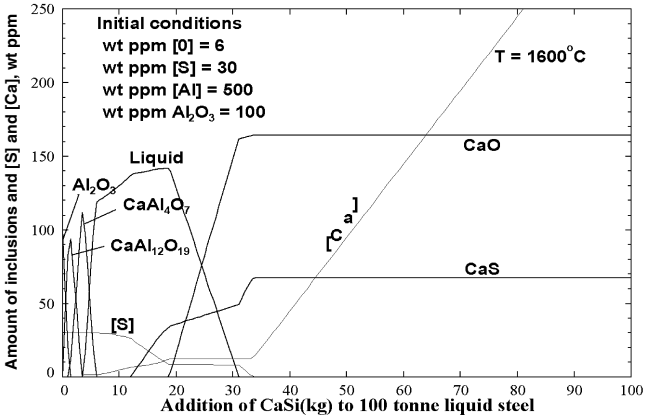

(a)

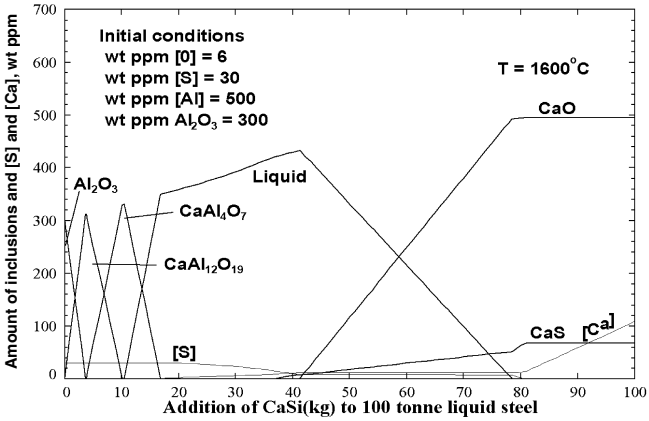

(b)

Figure 23. Modification of Al_2O_3 inclusions and variation of total dissolved [Ca] and [S] content of steel with CaSi injection into 100 tonnes of Al deoxidized liquid steel containing sulphur at 1600°C. (a) Initial steel: [0]=6 ppm, [S]=30 ppm, [Al]=500 ppm and Al_2O_3=100 ppm; (b) Initial steel: [0]=6 ppm, [S]=30 ppm, [Al]=500 ppm and Al_2O_3=300 ppm

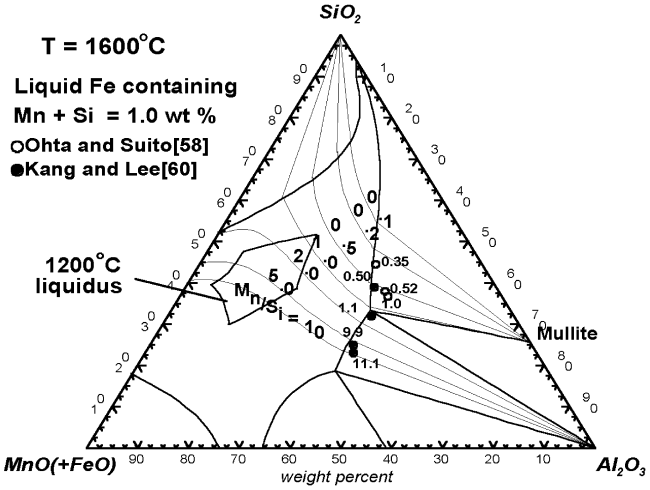

Figure 24. Calculated compositional trajectories of $MnO-Al_2O_3-SiO_2$ inclusions in equilibrium with liquid Fe containing various dissolved Mn/Si weight ratios and a total dissolved (Mn + Si) content of 1.0 wt% at 1600°C. Experimental[58,60] Mn/Si ratios at alumina or mullite saturation are shown beside each experimental point. The calculated liquidus curves at 1600°C and 1200°C are also shown

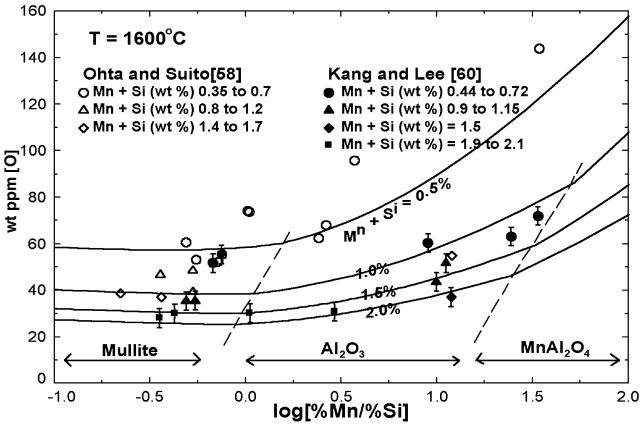

Figure 25. Calculated oxygen content versus dissolved Mn/Si weight ratio at various total dissolved (Mn + Si) contents in liquid Fe in equilibrium with liquid $MnO-Al_2O_3-SiO_2$ inclusions saturated with $MnAl_2O_4$, Al_2O_3, or mullite at 1600°C

In Figure 25 the measured oxygen contents of the steel at equilibrium simultaneously with liquid oxide and a solid oxide (i.e. along the phase boundaries of Figure 24) are plotted as functions of the Mn/Si ratio in the steel and are compared to the calculated curves. The experimental results exhibit a large amount of scatter. Agreement between the measurements and the calculations is within the experimental error limits.

The main interest in Mn/Si deoxidation is in maintaining the inclusions in the liquid state at the temperature of the wire production process (at 1200°C for tire-cord steel). Therefore, the liquidus curve of the $MnO-Al_2O_3-SiO_2$ system at 1200°C is superimposed on the diagram in Figure 24. The targeted inclusion compositions should lie inside the 1200°C isotherm. Additional calculations show that the positions of the iso-Mn/Si lines are nearly independent of the total (Mn + Si) content. Furthermore, the calculated positions of these lines at 1550°C (which is near the solidification temperature of the steel) are nearly the same as at 1600°C. Thus it can be seen from Figure 24 that the Mn/Si weight ratio of the steel should be controlled to within the approximate limits: $1 < Mn/Si < 10$. Such diagrams permit one to target the appropriate ranges of Mn, Si and Al in steel to maintain the inclusions in the liquid state.

Conclusions

Extensive computerized thermodynamic databases have been prepared for solid and liquid oxide phases and for solid and liquid steel and carbonitride phases. These databases have been developed by critical evaluation of all available thermodynamic and phase diagram data through the use of models appropriate to the structure of each solution. The models reproduce all experimental data within experimental error limits and permit good estimations to be made of the thermodynamic properties of multicomponent solutions based on the evaluated and optimized model parameters of lower-order (binary and ternary) subsystems. Modern Gibbs energy minimization software is used to access these databases automatically and calculate the conditions for equilibrium in multicomponent, multiphase systems.

Several examples have been presented in which such calculations are used to elucidate and predict complex

equilibria involving inclusion formation at various stages of steelmaking. The use of thermodynamic calculations can reduce costs and aid in the development of new technology. Furthermore, the combination of thermodynamic calculations and process modelling should result in advances in the automation of steelmaking processes.

Acknowledgments

This project was supported by a CRD grant from the Natural Sciences and Engineering Research Council of Canada in collaboration with the following: INCO, Noranda, Rio Tinto, TeckCominco, Alcoa, Dupont, Shell, Corning, Pechiney, Norsk Hydro, Sintef, Schott Glas, St.-Gobain Recherche, Mintek, and IIS Materials.

References

1. FactSage, Ecole Polytechnique, Montréal, http://www.factsage.com/, 2002.
2. PELTON, A.D. and BLANDER, M. Thermodynamic Analysis of Ordered Liquid Solutions by a Modified Quasi-Chemical Approach. Application to Silicate Slags. *Metall. Trans. B*, vol. 17B. 1986. pp. 805–815.
3. PELTON, A.D., DECTEROV, S.A., ERIKSSON, G., ROBELIN, C., and DESSUREAULT, Y. The Modified Quasichemical Model. I—Binary Solutions. *Metall. Mater. Trans. B*, vol. 31B. 2000. pp. 651–659.
4. PELTON, A.D. and CHARTRAND, P. The Modified Quasichemical Model. II—Multicomponent Solutions. *Metall. Mater. Trans. A*, vol. 32A. 2001. pp. 1355-1360.
5. HILLERT, M., JANSSON, B., and SUNDMAN, B. Application of the Compound-Energy Model to Oxide Systems. *Z. Metallkd.*, vol. 79, no. 2. 1988. pp. 81–87.
6. DECTEROV, S.A., JAK, E., HAYES, P.C., and PELTON, A.D. Experimental Study of Phase Equilibria and Thermodynamic Optimization of the Fe-Zn-O System. *Metall. Mater. Trans. B.,* vol. 32 B, no. 4. 2001. pp. 643–657.
7. PELTON, A.D. Thermodynamic Calculations of Chemical Solubilities of Gases in Oxide Melts and Glasses. *Glastech. Ber.*, vol. 72, no. 7. 1999. pp. 214–226.
8. PELTON, A.D., ERIKSSON, G., and ROMERO-SERRANO, A. Calculation of Sulfide Capacities of Multicomponent Slags. *Metall. Trans. B*, vol. 24B. 1993. pp. 817–825.
9. JUNG, I.-H., DECTEROV, S.A., and PELTON, A.D. A Thermodynamic Model for Deoxidation Equilibria in Steel. *Metall. Mater. Trans.*, accepted. 2003.
10. SPENCER, P. personal communication. 2003.
11. Scientific Group Thermodata Europe. http://www.sgte.org/. 2002.
12. ERIKSSON, G. and PELTON, A.D. Critical Evaluation and Optimization of the Thermodynamic Properties and Phase Diagrams of the CaO-Al_2O_3, Al_2O_3-SiO_2, and CaO-Al_2O_3-SiO_2 Systems. *Metall. Trans.*, vol. 24B. 1993. pp. 807–816.
13. GREIG, J.W. Immiscibility in Silicate Melts. Part I. *Am. J. Sci.*, 5th Series, vol. 13, no. 73. 1927. pp. 1–44.
14. SCHUHMANN, R., POWELL, R.G., and MICHAL, E.J. Constitution of the FeO-Fe_2O_3-SiO_2 System at Slag-Making Temperatures. *Trans AIME, J. Metals*, vol. 197. 1953. pp. 1097–1104.
15. BOWEN, N.L. and SCHAIRER, J.F. The System FeO-SiO_2. *Am. J. Sci.*, (5th Series), vol. 24, no. 5. 1932. pp. 177–213.
16. GREIG, J.W. On Liquid Immiscibility in the System FeO-Fe_2O_3-Al_2O_3-SiO_2. *Am. J. Sci.*, (5th Series), vol. 14, no. 5. 1927. pp. 473–84.
17. ALLEN, W.C. and SNOW, R.B. The Orthosilicate-Iron Oxide Portion of the System CaO-'FeO'-SiO_2. *J. Am. Ceram. Soc.*, vol. 38. 1955. pp. 264–280.
18. SCHUHMANN, R. and ENSIO, P.J. Thermodynamics of Iron-Silicate Slags: Slags Saturated with Gamma Iron. *Trans. AIME, J. Metals*, vol. 3. 1951. pp. 401–411.
19. MUAN, A. Phase Equilibria in the System FeO-Fe_2O_3-SiO_2. *Trans. Metall. Soc. AIME*, vol. 203. 1955. p. 965.
20. ABBATTISTA, F., BURDESE, A., and MAJA, M. Equilibrium Diagrams of CaO-FeO_x System. *Rev. Int. Hautes Temp. Refract.*, vol. 12. 1975. pp. 337–342.
21. LARSON, H. and CHIPMAN, J. Oxygen Activity in Iron Oxide Slags. *Trans. AIME, J. Met.*, vol. 197. 1953. pp. 1089–1096.
22. TAKEDA, Y., NAKAZAWA, S., and YAZAWA, A. Thermodynamics of Calcium Ferrite Slags at 1200°C and 1300°C. *Can. Metall. Q.*, vol. 19, no. 3. 1980. pp. 297–305.
23. TIMUCIN, M. and MORRIS, A.E. Phase Equilibria and Thermodynamic Studies in the System CaO-FeO-Fe_2O_3-SiO_2. *Metall. Trans.*, vol. 1. 1970. pp. 3193–3201.
24. PHILLIPS, B. and MUAN, A. Phase Equilibria in the System CaO-Iron Oxide in Air and at 1 atm O_2 Pressure. *J. Am. Ceram. Soc.*, vol. 41, no. 11. 1958. pp. 445–454.
25. HARA, S., ARAKI, T., and OGINO, K. *Metall.Slags Fluxes. Int. Symp. Proc. 2nd*, 1984. Fine H.A. and Gaskell D.R. (eds.). Metall. Soc. AIME, Warrendale, 1984. pp. 441–451.
26. FISCHER, V.A. and HOFFMANN, A.H. Das Zustandsschaubild Eisenoxydul-Aluminiumoxyd. Arch. *Eisenhuettenwes.*, vol. 27, no. 5. 1956. pp. 343–346.
27. TURNOCK, A.C. and EUGSTER, H.P. Fe-Al Oxides: Phase Relationsships below 1000°C. *J. Petrol.*, vol. 3, no. 3. 1962. pp. 533–565.
28. NOVOKHATSKII, I.A., BELOV, B. F., GOROKH, A. V., and SAVINSKAYA, A.A. The Phase Diagram for The System Ferrous Oxide-Alumina. *Russ. J. Phys. Chem.*, vol. 39, no. 11. 1965. pp. 1498–1500.
29. ROSENBACH, K. and SCHMITZ, J.A. Ternary System Iron(II) Oxide-Chromium(III) Oxide-Alumina. *Arch. Eisenhuettenwes.*, vol. 45, no. 12. 1974. pp. 843–847.
30. HAY, R., MCINTOSH, A.B., RAIT, J., and WHITE, R.J. Slag Systems. *J. West Scot. Iron Steel Inst.*, vol. 44. 1936/1937. pp. 85–92.
31. ATLAS, L.M. and SUMIDA, W.K. Solidus, Subsolidus, and Subdissociation Phase Equilibria in the System Fe-Al-O. *J. Am. Ceram. Soc.*, vol. 41, no. 5. 1958. pp. 150–160.
32. OELSEN, W. and HEYNERT, G. Die Reaktionen

zwischen Eisen-Mangan-Schmelzen und den Schmelzen ihrer Aluminate. *Arch. Eisenhuettenwes.*, vol. 26, no. 10. 1955. pp. 567-575.

33. ELREFAIE, F.A. and SMELTZER, W.W. Thermodynamics of the System Iron-Aluminium-Oxygen between 1073 and 1573 K. *Metall. Trans. B*, vol. 14B. 1983. pp. 85–92.

34. RICHARDS, R.G. and WHITE, J. Phase Relationship of Iron-Oxide-Containing Spinels. *Trans. Brit. Ceram. Soc.*, vol. 53. 1954. p. 233.

35. MUAN, A. and GEE, C.L. Phase Equilibrium Studies in the System Iron Oxide-Al_2O_3 in Air and at 1 Atm. O_2 Pressure. *J. Am. Ceram. Soc.*, vol. 39. 1956 p. 207.

36. ROITER, B.D. Phase Equilibria in the Spinel Region of the System FeO-Fe_2O_3-Al_2O_3. *J. Am. Ceram. Soc.*, vol. 47, no. 1. 1964. pp. 509–511.

37. MEYERS, C., MASON, T.O., PETUSKEY, W.T., HALLORAN, J.W., and BROWN, J.K. Phase Equilibria in the System Fe-Al-O. *J. Am. Ceram. Soc.*, vol. 63, no. 11–12. 1980. pp. 659–663.

38. BOWEN, N.L., SCHAIRER, J.F., and PSNJAK, E. The System CaO-FeO-SiO_2. *Am. J. Sci.*, vol. 26. 1933. pp. 191–284.

39. BURDICK, M.D. Studies on the System Lime-Ferric Oxide-Silica. *J. Res. Nat. Bur. Stand.*, US Dept. of Commerce, Research paper RP1340, vol. 25. 1940. pp. 475–488.

40. ZHANG, H., YE, D., ZHANG, P., and CHEN, X. Influence of Lime (20 wt pct) on the Liquid Field of the System FeO-$FeO_{1.5}$-SiO_2. *Zhongnan Kuangye Xueyuan Xuebao*, vol. 21, no. 4. 1990. pp. 447–450.

41. PHILLIPS, B. and MUAN, A. Phase Equilibria in the System CaO-Iron Oxide-SiO_2 in Air. *J. Am. Ceram. Soc.*, vol. 42, no. 9. 1959. pp. 413–423.

42. DAYAL, R.R. and GLASSER, F.P. Phase Relations in the System CaO-Al_2O_3-Fe_2O_3. Sci of Cer-cs, vol. 3, G.H.Stewart, (ed.) *Academic Press Inc.* (Ltd.), London, vol. 3. 1967. pp. 191–214.

43. NEWKIRK, T.F. and THWAITE, R.D. Pseudoternary System Calcium Oxide-Monocalcium Aluminate ($CaO.Al_2O_3$)-Dicalcium Ferrite ($2CaO.Fe_2O_3$). *J. Res. Nat. Bur. Stand.*, vol. 61, no. 4. 1958. pp. 233–245.

44. SWAYZE, M.N. Report on Studies of the Ternary System CaO-C_5A_3-C_2F; The Quaternary System CaO-C_5A_3-C_2F-C_2S; The Quaternary System as Modified by 5% MgO. *Am. J. Sci.*, vol. 244, no. 2. 1946. pp. 65–94.

45. ZHAO, B., JAK, E., and HAYES, P. personal communication. 2003.

46. GÖRL, E., OETERS, F., and SCHEEL, R. Balances between Hot Metal and Saturated Slags of the CaO-FeOn-SiO_2 System, Taken with Sulphur Distribution. *Arch. Eisenhuettenwes.*, vol. 37, no. 6. 1966. pp. 441–445.

47. ERIKSSON, G., WU, P., BLANDER, M., and PELTON, A.D. Critical Evaluation and Optimisation of the Thermodynamic Properties and Phase Diagrams of the MnO-SiO_2 and CaO-SiO_2 Systems. *Can. Metall. Q.*, vol. 33, no. 1. 1994. pp. 13–21.

48. WU, P., ERIKSSON, G., and PELTON, A.D. Critical Evaluation and Optimization of the Thermodynamic Properties and Phase Diagrams of the Calcia-Iron(II) Oxide, Calcia-Magnesia, Calcia-Manganese(II) Oxide, Iron(II) Oxide-Magnesia, Iron(II) Oxide-Manganese(II) Oxide, and Magnesia-Manganese(II) Oxide Systems. *J. Am. Ceram. Soc.*, vol. 76, no. 8. 1993. pp. 2065–2075.

49. JACOB, K.T. Revision of Thermodynamic Data on MnO-Al_2O_3 Melts. *Can. Metall. Q.*, vol. 20, no. 1. 1981. pp. 89–92.

50. TIMUCIN, M. and MUAN, A. Activity-Composition Relations in $NiAl_2O_4$-$MnAl_2O_4$ Solid Solutions and Stabilities of $NiAl_2O_4$ and $MnAl_2O_4$ at 1300 and 1400°C. *J. Am. Ceram. Soc.*, vol. 75. 1992. pp. 1399–1406.

51. LENEV, L.M. and NOVOKHATSKII, I.A. *Izvest. Akad. Nauk SSSR, Metal.*, vol. 3, no. 3. 1966. pp. 73–78.

52. DIMITROV, S., WEYL, A., and JANKE, D. *Steel Res.*, vol. 66. 1995. pp. 87–92.

53. ZHAO, Y., MORITA, K., and SANO, N. Thermodynamic Properties of the $MgAl_2O_4$-$MnAl_2O_4$ Spinel Solid Solution. *Met. Trans. B*, vol. 26B. 1995. pp. 1013–1017.

54. KIM, C.K. and McLEAN, A. Thermodynamics of Iron-Manganese Aluminate Spinel Inclusions in Steel. *Metall. Trans. B*, vol. 10B, no. 4. 1979. pp. 575–584.

55. BARIN, I. *Thermodynamic Data for Pure Substances*, VCH, Weinheim, Germany, 1989.

56. SHARMA, R.A. and RICHARDSON, F.D. Activities of Manganese Oxide, Sulfide Capacities, and Activity Coefficients in Aluminate and Silicate Melts. *Trans Metall. Soc. AIME*, vol. 233. 1965. pp. 1586–1592.

57. FUJISAWA, T. and SAKAO, H. Equilibrium between Manganese Oxide-Silicon-Dioxide-Aluminum Oxide-Iron(II) Oxide Slags and Liquid Steel. *Tetsu To Hagané*, vol. 63, no. 9. 1977. pp. 1504–11.

58. OHTA, H. and SUITO, H. Activities in MnO-SiO_2-Al_2O_3 Slags and Deoxidation Equilibria of Mn and Si. *Metall. Mater. Trans. B,* vol. 27B, no. 2. 1996. pp. 263–270.

59. ROGHANI, G., JAK, E., and HAYES, P. Phase Equilibrium Studies in the 'MnO'-Al_2O_3-SiO_2 System. *Metall. Mater. Trans. B*, vol. 33B, no. 6. 2002. pp. 827–838.

60. KANG, Y.-B. and LEE, H.-G. unpublished work.

61. SAKAO, H. *Tetsu to Hagané*, vol. 56. 1970. pp. S621–624.

62. WOO, D.-H., KANG, Y.-B., and LEE, H.-G. Thermodynamic Study of MnO-SiO_2-Al_2O_3 Slag System: Liquidus Lines and Activities of MnO at 1823 K. *Metall. Mater. Trans. B*, vol. 33B, no. 6. 2002. pp. 915–920.

63. DING, W. and OLSEN, S.E. *Scand. J. Metall.*, vol. 25. 1996. p. 232.

64. JUNG, I.-H., DECTEROV, S.A., and PELTON, A.D. Computer Applications of Thermodynamic Databases to Inclusion Engineering. *ISIJ Int.*, accepted.

65. SEO, J.-D. and KIM, S.-H. Bull. Kor. *Inst. Metall. Mater.* (Korea), vol. 12. 1999. p. 402.

66. GUSTAFSSON, S. and MELLBERG, P.O. *Scand. J. Metall.*, vol. 9. 1980. p. 111.

67. OTOTANI, T., KATAURA, Y., and DEGAWA, T. *Trans. Iron Steel Inst*., Japan, vol. 16. 1976. p. 275.

68. MIYASHITA, Y. and NISHIKAWA, K. T*etsu to Hagané*, vol. 57. 1971. p. 1969.

69. HAN, Q., ZHANG, X., CHEN, D., and WANG, P. *Metall. Trans. B*, vol. 19B. 1988. p. 617.

70. OZAWA, M. *The Japan Society for the Promotion of Science, 19th Committee paper No. 9837*, Iron Steel Institute of Japan, Toyko. 1975. pp. 6.

71. Japan Society for the Promotion of Science, 19th Comm. On Steelmaking. *Steelmaking Data Sourcebook*, Gordon & Breach Science, New York, NY, 1988.

72. ITOH, H., HINO, M., and BAN-YA, S. *Metall. Mater. Trans. B*, vol. 28B. 1997. p. 953.

73. NADIF, M. and GATELLIER, C. Revue de *Metallurgie-CIT*, vol. 83. 1986. p. 277.

74. CHO, S.W. and SUITO, H. *ISIJ Int*., vol. 34. 1994. p. 265.

75. TURKDOGAN, E.T. *Steel Res*., vol. 62. 1991. p. 379.

76. GOKCEN, N.A. and CHIPMAN, J. Aliminum-Oxygen Equilibrium in Liquid Iron. *Trans. AIME* (Trans. Am. Inst. Mining Met. Eng.), vol. 194. 1953. pp. 173–178.

77. McLEAN, A. and BELL, H.B.J. *Iron Steel Inst*., vol. 203. 1965. pp. 123–130.

78. FRUEHAN, R.J. *Metall. Trans*., vol. 1. 1970. pp. 3403–3410.

79. JANKE, D. and FISHER, W.A. *Arch. Eisenhüttenw*., vol. 47. 1976. pp. 195–198.

80. DIMITROV, S., WEYL, A., and JANKE, D. *Steel Res*., vol. 66. 1995. pp. 3–7.

81. SEO, J.-D., KIM, S.-H., and LEE, K.-R. *Steel. Res.*, vol. 69. 1998. pp. 49–53.

82. SIGWORTH, G.K. and ELLIOTT, J.F. *Met. Sci.*, vol. 8. 1974. pp. 298-310.

83. LEE, K.R. and SUITO, H. Activities of Fe_tO in CaO-Al_2O_3-SiO_2-Fe_tO (<5 Pct) Slags Saturated with Liquid Iron. Metall. *Mater. Trans. B* , vol. 25B, no. 6. 1994. pp. 893–902.

84. SCHURMANN, E., BRAUN, U., and PLUSCHKELL, W. *Steel Res*., vol. 69. 1998. p. 355.

85. SUITO, H., INOUE, H., and INOUE, R. *ISIJ Int*., vol. 31. 1991. p. 1381.

86. ICHIHASHI, H. and IKEDA, T. Shape Control of Inclusions, *Committee on Non Inclusion Shape Control, Organization of Joint Society on Iron and Steel Basic Research*, Iron Steel Institute of Japan, Tokyo, 1984.

87. KIMURA, T. and SUITO, H. *Metall. Trans. B*, vol. 25B. 1994. p. 33.

88. OHTA, H. and SUITO, H. Deoxidation Equilibria of Calcium and Magnesium in Liquid Iron. *Metall. Mater. Trans. B*, vol. 28B. 1997. pp. 1131–1139.

89. FAULRING, G.M. and RAMALINGAM, S. Inclusion Precipitation Diagram for the Iron-Oxygen-Calcium-Aluminum System. *Metall. Trans. B*, vol. 11B, no. 1. 1980. pp. 125–30.

90. TURKDOGAN, E.T. *Second International Conference on Clean Steel*. Balatonfüred, Hungary, 1981. p. 3.

91. GATELLIER, C., GAYE, H., and NADIT, M. *Second International Conference on Clean Steel.* Balatonfüred, Hungary, 1981. p. 31.

92. LE, T.T. and ICHIKAWA, M. *Proceedings of the Second Canada-Japan Symposium on Modern Steelmaking and Casting Techniques*. CIM, Toronto, 1994. p. 29.